

Magnetic-Field-Induced Spin Nematicity in $\text{FeSe}_{1-x}\text{S}_x$ and $\text{FeSe}_{1-y}\text{Te}_y$ Superconductor Systems

Shaobo Liu^{1,2}, Jie Yuan^{1,3,4}, Sheng Ma^{1,2}, Zouyouwei Lu^{1,2}, Yuhang Zhang^{1,2}, Mingwei Ma^{1,4}, Hua Zhang^{1,2}, Kui Jin^{1,2,3,4}, Li Yu^{1,2,4}, Fang Zhou^{1,2,4*}, Xiaoli Dong^{1,2,3,4*}, and Zhongxian Zhao^{1,2,3,4}

¹ *Beijing National Laboratory for Condensed Matter Physics and Institute of Physics, Chinese Academy of Sciences, Beijing 100190, China*

² *School of Physical Sciences, University of Chinese Academy of Sciences, Beijing 100049, China*

³ *Key Laboratory for Vacuum Physics, University of Chinese Academy of Sciences, Beijing 100049, China*

⁴ *Songshan Lake Materials Laboratory, Dongguan, Guangdong 523808, China*

* Correspondence to: fzhou@iphy.ac.cn (F.Z.); dong@iphy.ac.cn (X.D.)

Abstract

The angular-dependent magnetoresistance (AMR) of the ab plane is measured on the single crystals of $\text{FeSe}_{1-x}\text{S}_x$ ($x = 0, 0.07, 0.13$ and 1) and $\text{FeSe}_{1-y}\text{Te}_y$ ($y = 0.06, 0.61$ and 1) at various temperatures under fields up to 9 T. A pronounced twofold-anisotropic carrier-scattering effect is identified by AMR, and attributed to a magnetic-field-induced spin nematicity that emerges from the tetragonal normal-state regime below a characteristic temperature T_{sn} . This magnetically polarized spin nematicity is found to be ubiquitous in the isoelectronic $\text{FeSe}_{1-x}\text{S}_x$ and $\text{FeSe}_{1-y}\text{Te}_y$ systems, no matter whether the sample shows an electronic nematic order at $T_s \lesssim T_{\text{sn}}$, or an antiferromagnetic order at $T_N < T_{\text{sn}}$, or neither order. Importantly, we find that the isoelectronic substitution with sulfur does not suppress but even enhances the characteristic T_{sn} of the induced spin nematicity in $\text{FeSe}_{1-x}\text{S}_x$ samples. This contrasts sharply with their rapidly suppressed T_s , the transition temperature of the spontaneous electronic nematicity. Furthermore, we find that the superconductivity is significantly suppressed with the enhancement of the induced spin nematicity in both $\text{FeSe}_{1-x}\text{S}_x$ and $\text{FeSe}_{1-y}\text{Te}_y$ samples.

The superconductivity in iron-based compounds emerges as the antiferromagnetic (AFM) order in their metallic parent compounds is suppressed,^[1-4] analogous to the superconductivity in cuprates that is achieved by doping an AFM Mott insulator.^[5] This supports the AFM fluctuations as the driving force for electron pairing. In iron chalcogenide systems of $\text{FeSe}_{1-x}\text{S}_x\text{-FeSe}_{1-y}\text{Te}_y$, the binary parent compound FeTe (with $y = 1$ and presence of interstitial Fe) shows a double-stripe AFM order with a $(\sim\pi/2, \sim\pi/2)$ wave vector^[6-8] below $T_N = 60 - 75$ K.^[9-12] A dome-like superconducting (SC) regime appears upon suppression of the antiferromagnetism by substituting Se for Te.^[2,9,10] At the other end of the systems, no long-range AFM order but the presence of single-stripe $(\pi, 0)$ AFM fluctuations^[13] is observed in FeS ($x = 1$), which superconducts at $T_c \sim 5$ K.^[14] The intermediate FeSe ($x = 0$) with $T_c \sim 9$ K is unique in that, while in absence of an AFM order, it displays an electronic nematic order associated with a tetragonal to orthorhombic structural transition upon cooling to $T_s \sim 90$ K.^[15] This seems to raise a question that whether the pairing is mediated still by the AFM fluctuations or by the nematic fluctuations. Nevertheless, previous inelastic neutron scatterings of FeSe have revealed in its tetragonal regime the isotropic (π, π) Néel AFM fluctuations that coexist with the anisotropic $(\pi, 0)$ ones,^[16] and in its nematic regime the dominating stripe fluctuations.^[16-19] This crossover from the significant isotropic to dominating anisotropic AFM fluctuations with cooling also manifests itself in the macroscopic properties. For instance, in the in-plane angular-dependent magnetoresistance (AMR)^[20] and directional magnetic^[21] measurements, a twofold anisotropy has been observed to simultaneously appear at the nematic transition of FeSe. Recently, nuclear magnetic resonance^[22] and theoretical^[23] studies of FeSe suggest a nematic state that involves not only the Fe d_{xz}/d_{yz} orbitals but may also the d_{xy} orbital, likely due to nontrivial spin-orbit coupling effect.^[22,24] On the other hand, recent experimental studies of isoelectronic $\text{FeSe}_{1-x}\text{S}_x\text{-FeSe}_{1-y}\text{Te}_y$ ^[25] and FeSe^[26] systems suggest that the physics in the tetragonal environment, *i.e.* beyond the electronic nematic regime, is fundamental for the origin of superconductivity. Further investigating how the AFM fluctuations evolve and affect the superconductivity in $\text{FeSe}_{1-x}\text{S}_x$ and $\text{FeSe}_{1-y}\text{Te}_y$ systems is highly desirable for a better understanding of the origin.

In this work, we systematically measure the angular-dependent magnetoresistance within the ab plane of the single crystal samples of $\text{FeSe}_{1-x}\text{S}_x$ ($x = 0, 0.07, 0.13, 1$) and $\text{FeSe}_{1-y}\text{Te}_y$ ($y = 0.06, 0.61, 1$). The in-plane AMR measurement has proved to be effective and efficient in probing the temperature-dependent anisotropy of spin correlations present in the layered iron-based compounds.^[20,27,28] As expected for the electronically nematic FeSe and magnetically double-stripe $\text{Fe}_{1.19}\text{Te}$, a pronounced twofold anisotropy in their AMR is observed below a characteristic temperature T_{sn} . While T_{sn} coincides with T_s of the nematic electronic transition in FeSe, T_{sn} is found to be well above T_N of the double-stripe AFM transition in $\text{Fe}_{1.19}\text{Te}$. The similar twofold anisotropy has previously been identified by AMR in bulk Fe_{1-x}Se system and ascribed to the emergence of a magnetic-field-induced spin nematicity below T_{sn} .^[20] Interestingly, however, such a twofold-symmetric AMR is also identified here in the non-magnetic tetragonal FeS and FeSe_{1-}

$_y\text{Te}_y$ ($y = 0.06, 0.61$) samples. Importantly, we find that the isoelectronic substitution with sulfur does not suppress but even enhances T_{sn} of the induced spin nematicity in $\text{FeSe}_{1-x}\text{S}_x$ samples. This is in sharp contrast to their rapidly suppressed T_s of the spontaneous electronic nematicity. Furthermore, we find that T_c of the superconductivity is significantly suppressed with enhanced T_{sn} of the induced spin nematicity in both $\text{FeSe}_{1-x}\text{S}_x$ and $\text{FeSe}_{1-y}\text{Te}_y$ samples. We discuss this suppression of superconductivity within the AFM-fluctuation-driven pairing scenario.

The in-plane angular-dependent magnetoresistance and zero-field resistivity were measured on a Quantum Design PPMS-9 system with a four-probe configuration. The AMR data at various temperatures under magnetic fields (up to 9 T) parallel to the ab plane were obtained by rotating the single crystal samples about their c axis. The x-ray ϕ -scan experiments of the (103) plane were carried out at room temperature on a diffractometer (Rigaku SmartLab, 9 kW) equipped with two Ge (220) monochromators. Two series of the single crystal samples of $\text{FeSe}_{1-x}\text{S}_x$ ($x = 0, 0.07, 0.13, 1$) and $\text{FeSe}_{1-y}\text{Te}_y$ ($y = 0.06, 0.61, 1$) are studied here. For all the samples except for FeS, the crystal growth, phase identification, crystallographic characterization, chemical composition, and the electronic and superconducting properties have been reported elsewhere.^[25] The corresponding characterizations of FeS single crystal grown by a hydrothermal method^[29] are presented in Fig. S1 of the supplementary material (SM). The temperature-dependent scaled resistivity and the first derivative of AFM parent $\text{Fe}_{1.19}\text{Te}$ ($y = 1$) with $T_N \sim 59$ K are given in SM Fig. S2. Its antiferromagnetic and concomitant structural transition^[9,11,12] are manifest in the pronounced resistive anomaly at T_N (Fig. S2).

The relative directions of the in-plane magnetic field and electric current with respect to the tetragonal a or b axis (the diagonal directions of the Fe square lattice) in our AMR measurements were determined by the x-ray ϕ scans of (103) plane. The experimental uncertainty is usually about 5° . As seen from Figs. 1(a-c), the ϕ -scan data of three representative samples (FeS, FeSe, $\text{FeSe}_{0.39}\text{Te}_{0.61}$) exhibit four successive peaks with an equal interval of 90° , consistent with the C_4 lattice rotational symmetry. The similar ϕ -scan results are obtained in other $\text{FeSe}_{1-x}\text{S}_x$ ($x = 0.07$) and $\text{FeSe}_{1-y}\text{Te}_y$ ($y = 0.06, 1$) samples and given in Fig. S3. Here we define α as the angle between the current I and a (or b) axis, and θ as the angle between the field H and b (or a) axis, as schematically illustrated in Figs. 1(g) and 1(h) for two of the different current directions, $\alpha = 0^\circ$ and 45° , respectively. At current angle $\alpha = 45^\circ$, I is along the nearest-neighbour (NN) Fe-Fe direction, with field angle $\theta = 45^\circ$ (or 225° etc.) corresponding to $H//I$. At $\alpha = 0^\circ$, I is along the next NN (NNN) Fe-Fe direction, with $\theta = 0^\circ$ (or 180° etc.) corresponding to $H \perp I$.

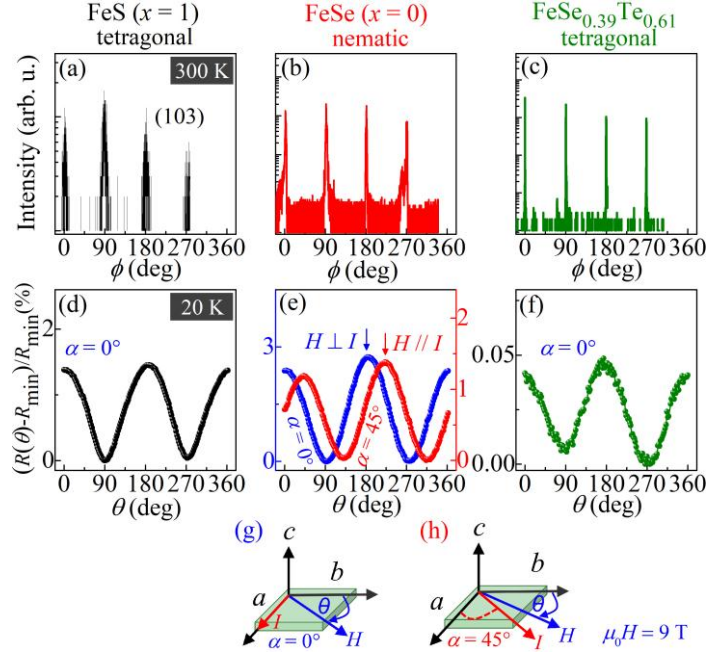


Fig. 1. The results of room-temperature x-ray ϕ scans of (103) plane for (a) FeS, (b) FeSe, and (c) FeSe_{0.39}Te_{0.61} agree with the C_4 lattice rotational symmetry and are used to calibrate the relative orientations of AMR measurements. The data of anisotropic AMR measured at temperature of 20 K and magnetic field of 9 T are presented here as the ratios of $\Delta R(\theta)/R_{\min}$ for (d) tetragonal FeS, (e) nematic FeSe, and (f) tetragonal FeSe_{0.39}Te_{0.61}. Two of the different configurations of AMR measurement, with the current angle $\alpha = 0^\circ$ (g) and 45° (h), are schematically illustrated.

In Figs. 1(d-f), the AMR results at the low temperature $T = 20$ K and the magnetic field $\mu_0 H = 9$ T are presented as the ratios of $\Delta R(\theta)/R_{\min} = [R(\theta) - R_{\min}]/R_{\min} \times 100\%$ for the three samples. Here R_{\min} is the minimum resistance when the magnetic field rotates from $\theta = 0^\circ$ to 360° . The twofold anisotropy in AMR is evident. This C_2 rotational symmetry in all our samples is noticeable from the polar plots of their $\Delta R(\theta, T)/R_{\min}(T)$ shown in Fig. 2, with Figs. 2(a) and 2(b-d) being the data for tetragonal ($x = 1$) and nematic ($x = 0, 0.07, 0.13$) FeSe_{1-x}S_x samples, respectively, Figs. 2(e) ($y = 0.06$) and 2(f) ($y = 0.61$) for tetragonal FeSe_{1-y}Te_y, and Fig. 2(g) for AFM parent Fe_{1.19}Te ($y = 1$). We emphasize that the twofold-symmetric AMR emerges no matter whether the system is nematically ordered (*e.g.* FeSe, with C_4 to C_2 symmetry breaking at T_s), or magnetically ordered (Fe_{1.19}Te, with C_4 symmetry broken at T_N), or show neither of the orders (*e.g.* FeS and FeSe_{0.39}Te_{0.61}, with persistent C_4 lattice symmetry). The presence or absence of the electronic nematicity in the samples has been characterized in our recent study.^[25]

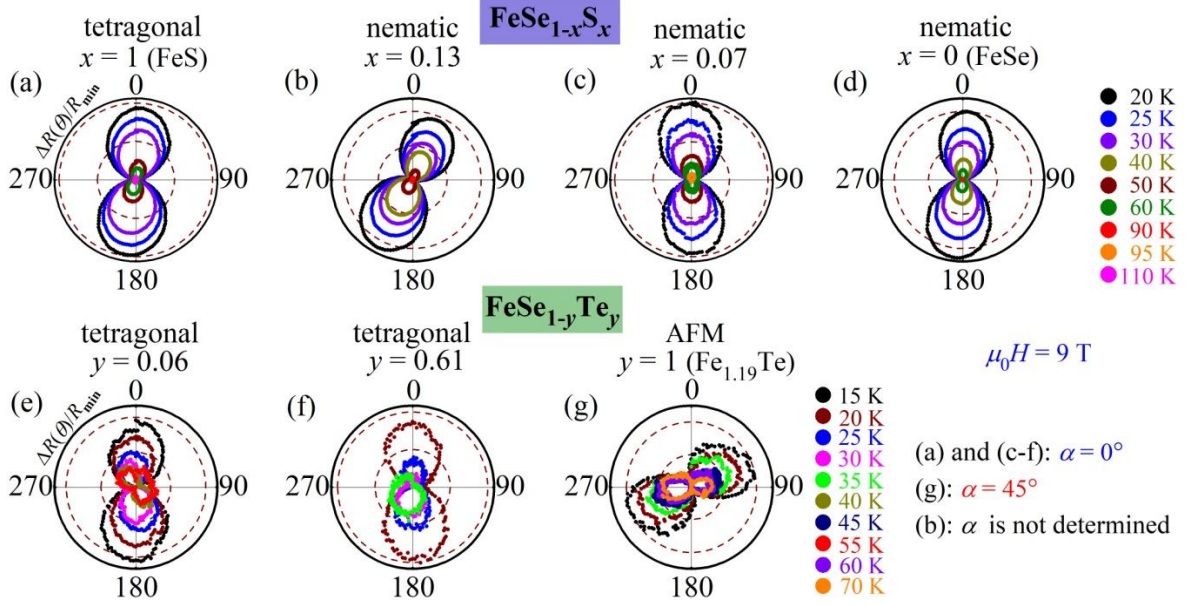


Fig. 2. The polar plots of $\Delta R(\theta, T)/R_{\min}(T)$ measured under magnetic field of 9 T for (a-d) $\text{FeSe}_{1-x}\text{S}_x$ ($x = 1, 0.13, 0.07, 0$) and (e-g) $\text{FeSe}_{1-y}\text{Te}_y$ ($y = 0.06, 0.61, 1$) samples. The current angle is $\alpha = 0^\circ$ for (a) and (c-f), and $\alpha = 45^\circ$ for (g). For $x = 0.13$ in (b), the relative orientation of AMR measurement was not checked by x-ray ϕ scan. For AFM $\text{Fe}_{1.19}\text{Te}$ in (g), the field angle θ corresponding to the maximum AMR twists at $T \gtrsim 45$ K, with the twist angle increased to $\sim 40^\circ$ at $T = T_{\text{sn}} \sim 70$ K. See main text for discussion. In (a) and (d), the field angle $\theta \sim 5^\circ$ corresponds to $H \perp I$. This angle off-set from $\theta = 0^\circ$ is due to the experimental uncertainty in setting up the rotating rod.

In order to quantify the temperature-dependent crossover from the isotropic to anisotropic carrier scatterings, we performed the AMR measurements at various temperatures. In Figs. 3(a-d) and 3(e-g), we present the temperature dependences of the maximum $\Delta R(T)/R_{\min}(T)$ of AMR at the field of 9 T for the two series of samples of $\text{FeSe}_{1-x}\text{S}_x$ ($x = 0, 0.07, 0.13, 1$) and $\text{FeSe}_{1-y}\text{Te}_y$ ($y = 0.06, 0.61, 1$), respectively. It is obvious that the twofold anisotropy in AMR develops below a well-defined characteristic temperature T_{sn} , and this anisotropy becomes strongly enhanced as the temperature is further lowered. In FeSe , it happens that T_{sn} (~ 90 K) coincides with T_{s} (~ 89 K) of its electronic nematicity, exactly the same as the previous AMR study of Fe_{1-x}Se system.^[20] In $\text{Fe}_{1.19}\text{Te}$, however, the anisotropic AMR is found to set in at a $T_{\text{sn}} \sim 70$ K well above $T_{\text{N}} \sim 59$ K of its double-stripe antiferromagnetism. Interestingly, in the non-magnetic tetragonal FeS with the lowest $T_{\text{c}} = 4.8$ K [Fig. S1(c)], the twofold-symmetric AMR is identified below a T_{sn} as high as 110 K. This $T_{\text{sn}} \sim 110$ K is far above the measuring temperature (4 K) of the neutron scatterings revealing the single-stripe AFM fluctuations.^[13] In the non-magnetic tetragonal $\text{FeSe}_{1-y}\text{Te}_y$, the twofold symmetry is observed below $T_{\text{sn}} \sim 40$ K for $y = 0.06$ ($T_{\text{c}} = 6.7$ K) and $T_{\text{sn}} \sim 30$ K for $y = 0.61$ ($T_{\text{c}} = 14$ K). We note that, although the AMR anisotropy of $\text{FeSe}_{1-y}\text{Te}_y$ is similarly pronounced to that of $\text{FeSe}_{1-x}\text{S}_x$, differences exist between them. The T_{sn} ($\lesssim 70$ K) of $\text{FeSe}_{1-y}\text{Te}_y$ samples is found to be much lower than the T_{sn} ($\gtrsim 90$ K) of $\text{FeSe}_{1-x}\text{S}_x$ samples. Moreover, $\text{FeSe}_{1-y}\text{Te}_y$ samples [Figs. 3(e-g)] exhibit the anisotropic AMR signals about one to two orders of magnitude weaker

than those of $\text{FeSe}_{1-x}\text{S}_x$ samples [Figs. 3(a–d)], despite having their much sharper isotropic-to-anisotropic crossover at T_{sn} than $\text{FeSe}_{1-x}\text{S}_x$ samples. These phenomena could be related to the facts that $\text{FeSe}_{1-y}\text{Te}_y$ is derived from parent $\text{Fe}_{1.19}\text{Te}$ with the complex double-stripe antiferromagnetism and magnetic frustrations,^[8] and both isotropic and anisotropic AFM fluctuations are present in substituted $\text{FeSe}_{1-y}\text{Te}_y$ (at, *e.g.*, $y = 0.62$), as revealed by the neutron scatterings.^[2] In Figs. 3(a–g), the temperature regions of the twofold-anisotropic AMR, electronic nematicity, and double-stripe antiferromagnetism are marked by the pink, purplish-blue, and green shadings, respectively. Particularly for FeSe in Fig. 3(d), the coexisting Néel and stripe AFM fluctuations in the tetragonal regime,^[16] as well as the dominating stripe ones in the nematic regime,^[16–19] as revealed by the previous neutron study are also indicated. Additionally, three of the neutron-scattering temperatures for FeSe^[16] and FeS^[13] are indicated in Fig. 4.

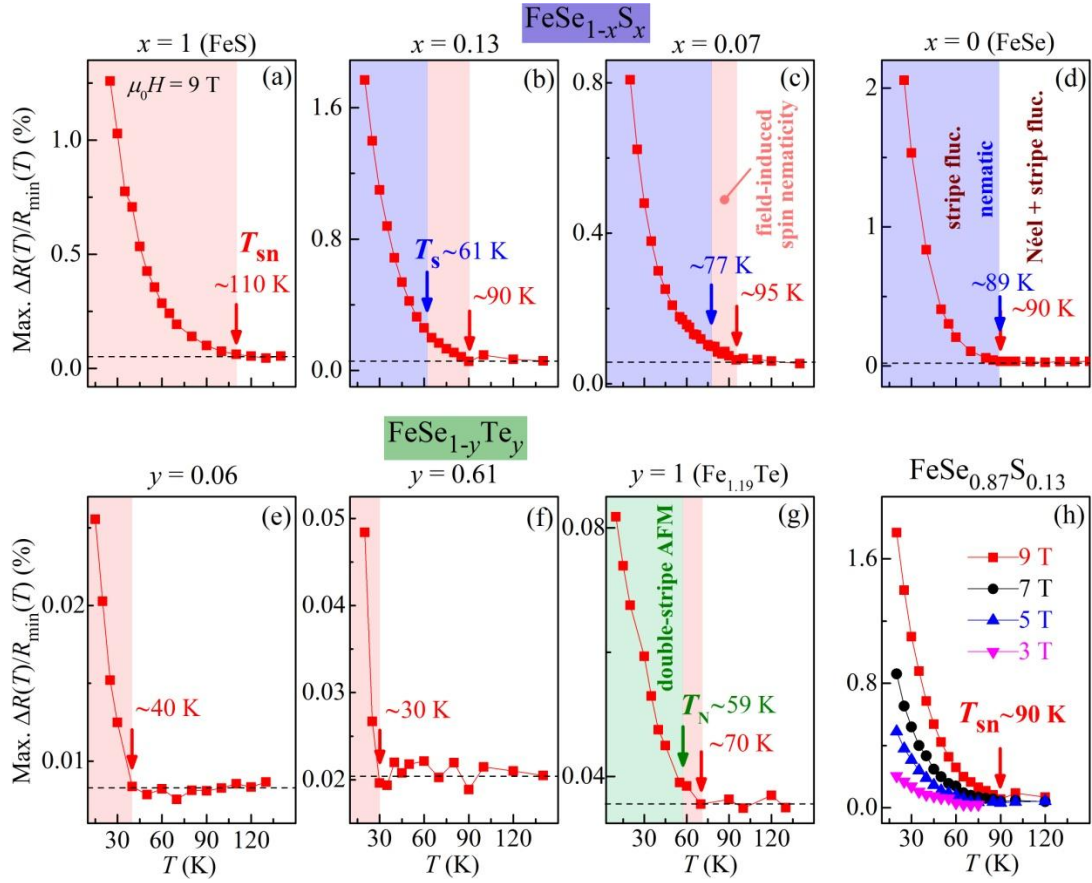


Fig. 3. (a–d) and (e–g) show the temperature dependences of the maximum $\Delta R(T)/R_{\text{min}}(T)$ of anisotropic AMR at the magnetic field of 9 T for $\text{FeSe}_{1-x}\text{S}_x$ ($x = 1, 0.13, 0.07, 0$) and $\text{FeSe}_{1-y}\text{Te}_y$ ($y = 0.06, 0.61, 1$) samples, respectively. The temperatures of T_{sn} , T_s , and T_N are indicated by the red, blue, and green arrows, respectively. The coexisting Néel and stripe AFM fluctuations in the tetragonal regime,^[16] as well as the dominating stripe ones in the nematic regime,^[16–19] are also indicated in (d) for FeSe. (h) The temperature-dependent maximum $\Delta R(T)/R_{\text{min}}(T)$ measured under various fields from 3 to 9 T for nematic $\text{FeSe}_{0.87}\text{S}_{0.13}$ ($x = 0.13$). (See Fig. S5 for the extracted field dependences of the maximum $\Delta R(T)/R_{\text{min}}(T)$ at given T 's < T_{sn} .)

The reproducibility of the twofold-symmetric AMR at $T < T_{\text{sn}}$ was also checked out at different current directions (α 's) on FeSe. Fig. 1(e) shows the results obtained with the configurations of current $\alpha = 0^\circ$ and 45° . The results obtained on one and the same sample at $\alpha = 0^\circ, 22^\circ$ and 90° are given in Fig. S4. The C_2 symmetry of AMR is well reproducible regardless of the different current directions. At the current $\alpha = 0^\circ$ or 90° (the NNN Fe-Fe directions), the maximum and minimum of $\Delta R(\theta, T)/R_{\text{min}}(T)$ are reached with $H \perp I$ and $H // I$, respectively, when H is parallel to the orthogonal NNN Fe-Fe directions [see Figs. 1(e, g)/S4(c, f) for $\alpha = 0^\circ$ with the corresponding field θ 's = 180° (maximum) and 90° (minimum), and S4(b, e) for $\alpha = 90^\circ$]. Additionally, at the current $\alpha = 22^\circ$ closer to the NNN Fe-Fe direction, as shown in Figs. S4(a, d), $\Delta R(\theta, T)/R_{\text{min}}(T)$ is maximized and minimized again when H is parallel to the orthogonal NNN Fe-Fe directions (with the θ 's = 180° and 90° , respectively), but the angles between H and I are changed to $\langle H, I \rangle = 90^\circ - 22^\circ$ and 22° , respectively (note that $\langle H, I \rangle = 90^\circ$ and 0° at $\alpha = 0^\circ$). However, a discontinuity is observed upon the current $\alpha = 45^\circ$, *i.e.* with I along the NN Fe-Fe direction. In this case [Figs. 1(e, h)], the maximum and minimum of $\Delta R(\theta, T)/R_{\text{min}}(T)$ are observed at the reversed $H // I$ and $H \perp I$ (as compared to the case of $\alpha = 0^\circ$), respectively, but not at $\langle H, I \rangle = 90^\circ - 45^\circ$ and 45° (as extrapolated from the cases of $\alpha = 0^\circ$ and 22°), when H is parallel to the orthogonal NN Fe-Fe directions [with the corresponding θ 's = 225° (or 45°) and 135° (= $225^\circ - 90^\circ$), respectively]. Here we first discuss the implication of the maximum/minimum carrier-scattering effects; the unusual change in the magnetic polarization effect due to the current-direction change from $\alpha = 0^\circ$ to 45° will be discussed later. In Fig. 1(e), the maximum and minimum scattering effects observed at $H \perp I$ and $H // I$, respectively, for $\alpha = 0^\circ$ imply that the directions of the spin arrays with the inherent antiferromagnetic/ferromagnetic (FM) correlations between neighboring spins are aligned by the magnetic field as being mainly perpendicular/parallel to H . But for $\alpha = 45^\circ$, the spin arrays are aligned by the field with the directions of the AFM/FM correlations between neighboring spins being mainly parallel/perpendicular to H , giving rise to the maximum and minimum scatterings at $H // I$ and $H \perp I$, respectively.

For the double-stripe AFM $\text{Fe}_{1.19}\text{Te}$ shown in Fig. 2(g), the maximum of its $\Delta R(\theta, T)/R_{\text{min}}(T)$ measured at current $\alpha = 45^\circ$ is observed at the field θ ($\sim 45^\circ$) almost in the NN Fe-Fe direction, *i.e.* with H almost parallel to I , at lower temperatures $\lesssim 45$ K. At higher temperatures $\gtrsim 45$ K, however, the maximum direction substantially deviates from the NN Fe-Fe direction by an angle up to $\sim 40^\circ$ (at $T = T_{\text{sn}} \sim 70$ K). Note that the temperature $T = 45$ K is well *below* $T_{\text{N}} \sim 59$ K. Such a large twist angle cannot be ascribed to the experimental uncertainty. This may be explained by the combined effects of the spin interactions (that are frustrated^[8]) and the magnetic polarization in $\text{Fe}_{1.19}\text{Te}$. When the spin correlation is strong, the magnetic field could only partially polarize the dominating anisotropic spin-correlated state. The polarization effect would change with temperature due to thermal fluctuations.

In our earlier AMR study of Fe_{1-x}Se system,^[20] the observed twofold-anisotropic scattering effect was attributed to a spin nematicity that is formed below T_{sn} due to the magnetic polarization effect, and an Ising-like order parameter was argued for the spin nematicity (see ref. 20 and the related references therein). In Fig. 3(h), the temperature dependences of maximum $\Delta R(T)/R_{\text{min}}(T)$ measured at various fields ≤ 9 T are plotted together for $x = 0.13$ FeSe_{0.87}S_{0.13}, which shows the electronic-nematic T_s (~ 61 K) much lower than the spin-nematic T_{sn} (~ 90 K). The magnetically induced nature of the spin nematicity is evident from Fig. 3(h). As the magnetic field strength is reduced, the twofold anisotropy in AMR at given $T < T_{\text{sn}}$ is correspondingly weakened. At the lower magnetic field of 3 T, the spin nematicity is just discernible by AMR. We note here that the appearance of the field-polarized spin nematicity in FeSe corresponds to the presence of dominating stripe AFM fluctuations at lower $T < T_s$ ($\sim T_{\text{sn}}$) as have been revealed by the neutron scatterings.^[16-19] And the disappearance of it above T_{sn} in turn corresponds to the presence of significant isotropic AFM fluctuations at higher $T > T_s$.^[16] The anisotropic spin fluctuations are also present in FeS^[13] and FeSe_{1-y}Te_y^[2,3] at low temperatures. The quickly increasing maximum $\Delta R(T)/R_{\text{min}}(T)$ with cooling as observed at lower $T < T_{\text{sn}}$ (Fig. 3) is consistent with the presence of the low- T anisotropic spin correlations. Moreover, the common twofold symmetry of AMR shared by all the FeSe_{1-x}S_x and FeSe_{1-y}Te_y samples suggests the common underlying physics. Nevertheless, as described and discussed above, there appear the unusual phenomena in AMR of FeSe. While the same characteristic feature of the magnetic polarizations is observed with current I along the orthogonal NNN Fe-Fe directions ($\alpha = 0^\circ$ or 90°), the polarization effects of field H on the AFM/FM spin arrays are found to be abruptly changed upon I along the NN Fe-Fe direction ($\alpha = 45^\circ$). The maximum scatterings at current $\alpha = 0^\circ$ and 90° can be interpreted as due to the field-aligned AFM spin arrays mainly perpendicular to H ($\perp I$), whereas those at $\alpha = 45^\circ$ as due to the field-aligned AFM spin arrays mainly parallel to H ($\parallel I$). This abrupt change appears to be difficult to comprehend if the induced spin nematicity is contributed purely and simply by Fe d_{xz}/d_{yz} orbitals, within the usual nematic picture. Therefore, such distinctly different magnetic polarization effects of spins observed at the currents along the nearest-neighbour ($\alpha = 45^\circ$) and next nearest-neighbour ($\alpha = 0^\circ/90^\circ$) Fe-Fe directions deserve further investigation by taking account of the orbital-selective effect. For instance, the in-plane-lying d_{xy} orbital may also be involved in the induced spin nematicity. Recent experiment^[22] and theory^[23] also suggest the possibility of d_{xy} contribution to nematicity.

Further, we recall that, in magnetically ordered iron pnictides SrFe₂As₂^[27] and BaFe_{2-x}Co_xAs₂^[28] with respective $T_N \sim 200$ K and 138 K (BaFe₂As₂ at $x = 0$), the similar C_2 -symmetric AMR was also observed and attributed to the occurrence of single-stripe antiferromagnetism commonly present in iron pnictides.^[30] Once the stripe AFM order has disappeared in BaFe_{2-x}Co_xAs₂ at $x > 0.2$, the twofold anisotropy in AMR simultaneously vanishes as well.^[28] On the other hand, previous neutron studies have detected the presence of local magnetic moments in FeS,^[13] FeSe,^[16] and FeSe_{0.65}Te_{0.35}^[31] systems without magnetic order, in addition to the itinerant contribution.

Moreover, an $S = 1$ paramagnet of FeSe,^[16] and nontrivial spin–orbit coupling effect in FeSe^[22,24] and FeSe_{0.5}Te_{0.5},^[32] have been suggested. Here, in the non-magnetic tetragonal FeS, the field-induced spin nematicity is significant at the high $T_{\text{sn}} \sim 110$ K so that it is well detectable by AMR. This is possibly due to that the crystal lattice of stoichiometric FeS is most contracted [see Fig. S1(b) and ref. 25], thus its interlayer coupling should be strongest among the FeSe_{1-x}S_x and FeSe_{1-y}Te_y systems. Although a long-range AFM order fails to establish in the FeSe_{1-x}S_x samples showing higher $T_{\text{sn}} (\gtrsim 90$ K) due to strongly frustrated magnetism,^[8,16,33-39] it indeed occurs in the strongly correlated parent Fe_{1.19}Te at T_{N} . However, T_{sn} (~ 70 K) of its induced spin nematicity is found to be well above T_{N} (~ 59 K) of its spontaneous double-stripe antiferromagnetism. This means that incipient anisotropic spin correlations have already well developed in Fe_{1.19}Te at higher $T = T_{\text{sn}}$ ($>T_{\text{N}}$) in the presence of spin-orbit coupling effect, as a precursor of the double-stripe order eventually occurring at lower $T = T_{\text{N}}$. Overall, the magnetic-field-induced spin nematicity is observed by AMR to be ubiquitous in FeSe_{1-x}S_x and FeSe_{1-y}Te_y systems, no matter whether the samples are nematically/magnetically ordered or not (Fig. 3). Therefore, it turns out that the enhancement of the anisotropy in AFM correlations below T_{sn} is an inherent property of the systems.

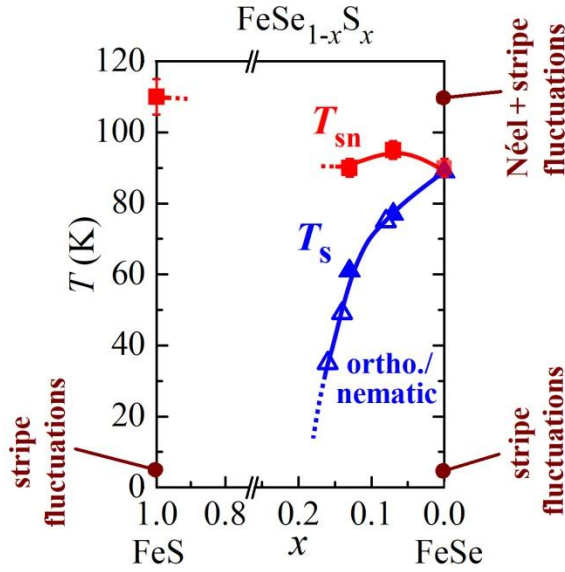


Fig. 4. Local phase diagram of T vs. x for FeSe_{1-x}S_x system. Here the data from ref. [40], as denoted by the hollow blue triangles, are also included. Three of the temperatures of previous neutron experiments of FeSe^[16] and FeS^[13] are marked.

Having identified the ubiquitous presence of the magnetically induced spin nematicity, now we switch to further discussion of the implication for superconductivity. First of all, as can be seen from the local phase diagram of FeSe_{1-x}S_x system plotted in Fig. 4, the isoelectronic substitution with sulfur strongly suppresses the electronic nematicity in FeSe_{1-x}S_x samples, with their T_{s} reduced from ~ 89 K ($x = 0$; $T_{\text{c}} = 8.5$ K), ~ 77 K ($x = 0.07$; $T_{\text{c}} = 10.3$ K), to ~ 61 K ($x = 0.13$; $T_{\text{c}} = 10.8$ K).^[25] In contrast, their spin-nematic T_{sn} is found to change little with substitution x (there is only a small

increase of T_{sn} by ~ 5 K at $x = 0.07$). As a result, T_{sn} of the induced spin nematicity is located well above T_{s} of the spontaneous electronic nematicity in the substituted $\text{FeSe}_{1-x}\text{S}_x$ ($0.13 \geq x > 0$) samples. Particularly in the left-end stoichiometric FeS with the maximized substitution ($x = 1$), the spin-nematic T_{sn} is even enhanced to ~ 110 K against the completely suppressed electronic nematicity. These experimental observations demonstrate that the isoelectronic sulfur substitution significantly reduces the electron-electron correlation due to the lattice contraction with increasing x [25,41,42] [see Fig. S1(b) for $x = 1$], hence it directly suppresses the spontaneous electronic nematicity, rather than the induced spin nematicity. In this sense, the spin-correlation channel is very likely separate from the electron-correlation channel.

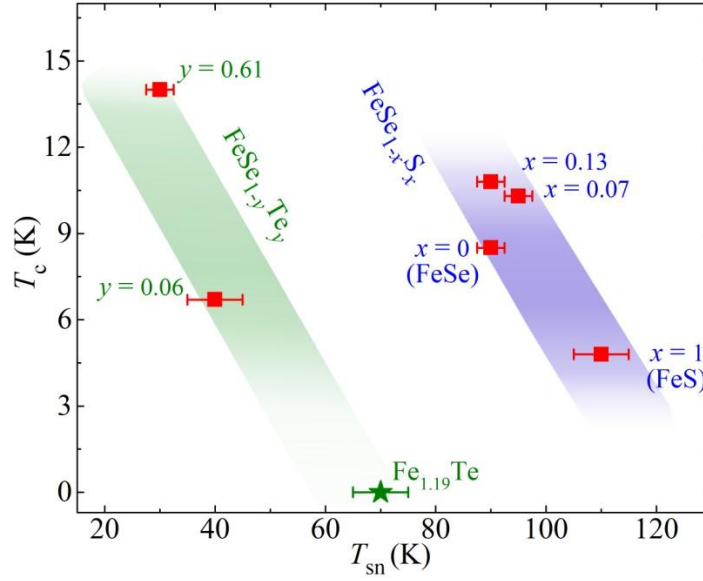


Fig. 5. T_c of the superconductivity vs. T_{sn} of the field-induced spin nematicity for isoelectronic $\text{FeSe}_{1-x}\text{S}_x$ and $\text{FeSe}_{1-y}\text{Te}_y$ samples. An anti-correlation between T_c and T_{sn} is revealed. The data of AFM parent $\text{Fe}_{1.19}\text{Te}$ is also included.

Furthermore, it is clear from Fig. 5 that the superconductivity is significantly suppressed with enhanced T_{sn} : The superconducting T_c is reduced from 14 K ($y = 0.61$) to 6.7 K ($y = 0.06$) in $\text{FeSe}_{1-y}\text{Te}_y$, and from 10.8 K ($x = 0.13$) to 4.8 K ($x = 1$) in $\text{FeSe}_{1-x}\text{S}_x$. Based on the related experimental observations and discussions above, one may take T_{sn} of the induced spin nematicity as a measure of the degree of anisotropy in AFM correlations to a certain extent. Thus, such a suppression of superconductivity implies that the enhanced anisotropy in AFM fluctuations undermines the superconductivity. This is also consistent with the enhancement of superconductivity in the presence of almost isotropic AFM fluctuations^[43,44] as observed in heavily electron-doped FeSe-based intercalate of $(\text{Li}, \text{Fe})\text{OHFeSe}$ ($T_c = 42$ K). In other words, the superconductivity is suppressed at least partly due to the reduced contributing pairing channels within the AFM-fluctuation-driven pairing mechanism.

On the other hand, it is worth mentioning that the suppression of superconductivity in these isoelectronic $\text{FeSe}_{1-x}\text{S}_x$ and $\text{FeSe}_{1-y}\text{Te}_y$ samples seemingly follows the reduction trend of the electron-electron correlation with increasing x or decreasing y as reported in previous studies.^[25,41,42] However, the previous studies have also shown that no persistent positive correlation between the superconductivity and electronic correlation exists in the whole regions of $\text{FeSe}_{1-x}\text{S}_x$ and $\text{FeSe}_{1-y}\text{Te}_y$ systems, since in general they display a non-monotonic variation of T_c against the continuous reduction of electronic correlation,^[25,41,42] though the positive correlation has been shown to hold for heavily electron-doped $\text{Rb}_{0.8}\text{Fe}_2(\text{Se}_{1-z}\text{S}_z)_2$ system.^[45] The superconductivity is enhanced to a high T_c (32 K) at moderate correlation in $\text{Rb}_{0.8}\text{Fe}_2(\text{Se}_{1-z}\text{S}_z)_2$.^[45] Additionally, in prototypical Fe_{1-x}Se and intercalated $(\text{Li, Fe})\text{OHFe}_{1-x}\text{Se}$ compounds, T_c has been reported as being suppressed with the increased hole doping associated with the Fe-deficiency x , due to the hole-doping x enhanced electronic correlations.^[46,47] Therefore, further investigations are required to clarify the complex effects of electronic correlations on the superconductivity in multi-orbital/band iron-based compounds. Nevertheless, an anti-correlation between the superconducting T_c and spin-nematic T_{sn} is observed in both $\text{FeSe}_{1-x}\text{S}_x$ and $\text{FeSe}_{1-y}\text{Te}_y$ samples (Fig. 5), and the spin correlation has been shown to be very likely separate from the electronic correlation with respect to the isoelectronic substitution in $\text{FeSe}_{1-x}\text{S}_x$ system (Fig. 4). Moreover, the induced spin nematicity is found to emerge basically from the tetragonal regime (Fig. 3). Therefore, we conclude that the spin-related physics that originates in the tetragonal regime, rather than the electronic nematic regime, underlies the superconductivity.

In summary, we show the ubiquitous presence of a spin nematicity in isoelectronic $\text{FeSe}_{1-x}\text{S}_x$ and $\text{FeSe}_{1-y}\text{Te}_y$ systems, based on systematic measurements of the angular-dependent magnetoresistance in the ab plane. This spin nematicity is induced by the in-plane magnetic field $\gtrsim 3$ T, and emerges from the tetragonal regime at a characteristic temperature T_{sn} , no matter whether the sample is ordered nematically at $T_s \lesssim T_{\text{sn}}$ or magnetically at $T_N < T_{\text{sn}}$, or shows neither of the orders. The issue of a possible involvement of Fe d_{xy} orbital, besides the d_{xz}/d_{yz} orbitals, in the induced spin nematicity is worthy of further investigation. Our results highlight that the isoelectronic substitution with sulfur directly suppresses the spontaneous electronic nematicity, rather than the induced spin nematicity, in $\text{FeSe}_{1-x}\text{S}_x$ system. Thus, the spin correlation is very likely separate from the electronic correlation to the certain extent. Furthermore, the enhancement of the induced spin nematicity leads to the significant suppression of the superconductivity. This implies that the enhanced anisotropy in AFM fluctuations undermines the superconductivity, consistent with the AFM-fluctuation-driven pairing scenario. These results provide new evidence that the spin-related physics originating from the tetragonal background is fundamental for the iron-based unconventional superconductivity.

We thank Profs Jiangping Hu and Kun Jiang for helpful discussions. This work is supported by the National Key Research and Development Program of China (Grant Nos. 2016YFA0300300 and 2017YFA0303003), the National Natural Science Foundation of China (Grant Nos. 12061131005, 11834016 and 11888101), the Strategic Priority Research Program of Chinese Academy of Sciences (Grant Nos. XDB25000000), and the Strategic Priority Research Program and Key Research Program of Frontier Sciences of the Chinese Academy of Sciences (Grant Nos. QYZDY-SSW-SLH001).

References

- [1] Zhao J, Huang Q, de la Cruz C, Li S L, Lynn J W, Chen Y, Green M A, Chen G F, Li G, Li Z, Luo J L, Wang N L and Dai P C 2008 *Nat. Mater.* **7** 953
- [2] Liu T J, Hu J, Qian B, Fobes D, Mao Z Q, Bao W, Reehuis M, Kimber S A J, Prokeš K, Matas S, Argyriou D N, Hiess A, Rotaru A, Pham H, Spinu L, Qiu Y, Thampy V, Savici A T, Rodriguez J A and Broholm C 2010 *Nat. Mater.* **9** 716
- [3] Lumsden M D, Christianson A D, Goremychkin E A, Nagler S E, Mook H A, Stone M B, Abernathy D L, Guidi T, MacDougall G J, de la Cruz C, Sefat A S, McGuire M A, Sales B C and Mandrus D 2010 *Nat. Phys.* **6** 182
- [4] Kasahara S, Shi H J, Hashimoto K, Tonegawa S, Mizukami Y, Shibauchi T, Sugimoto K, Fukuda T, Terashima T, Nevidomskyy A H and Matsuda Y 2012 *Nature* **486** 382
- [5] Lee P A, Nagaosa N and Wen X-G 2006 *Rev. Mod. Phys.* **78** 17
- [6] Ma F, Ji W, Hu J, Lu Z Y and Xiang T 2009 *Phys. Rev. Lett.* **102** 177003
- [7] Bao W, Qiu Y, Huang Q, Green M A, Zajdel P, Fitzsimmons M R, Zhernenkov M, Chang S, Fang M, Qian B, Vehstedt E K, Yang J, Pham H M, Spinu L and Mao Z Q 2009 *Phys. Rev. Lett.* **102** 247001
- [8] Glasbrenner J K, Mazin I I, Jeschke H O, Hirschfeld P J, Fernandes R M and Valentí R 2015 *Nat. Phys.* **11** 953
- [9] Fang M H, Pham H M, Qian B, Liu T J, Vehstedt E K, Liu Y, Spinu L and Mao Z Q 2008 *Phys. Rev. B* **78** 224503
- [10] Yeh K-W, Huang T-W, Huang Y-l, Chen T-K, Hsu F-C, M. Wu P, Lee Y-C, Chu Y-Y, Chen C-L, Luo J-Y, Yan D-C and Wu M-K 2008 *Europhys. Lett.* **84** 37002
- [11] Li S L, de la Cruz C, Huang Q, Chen Y, Lynn J W, Hu J P, Huang Y-L, Hsu F-C, Yeh K-W, Wu M-K and Dai P C 2009 *Phys. Rev. B* **79** 054503
- [12] Zaloznyak I A, Xu Z J, Wen J S, Tranquada J M, Gu G D, Solovyov V, Glazkov V N, Zheludev A I, Garlea V O and Stone M B 2012 *Phys. Rev. B* **85** 085105
- [13] Man H, Guo J G, Zhang R, Schönemann R, Yin Z P, Fu M X, Stone M B, Huang Q Z, Song Y, Wang W Y, Singh D J, Lochner F, Hickel T, Eremin I, Harriger L, Lynn J W, Broholm C, Balicas L, Si Q M and Dai P C 2017 *npj Quantum Mater.* **2** 14
- [14] Lai X F, Zhang H, Wang Y Q, Wang X, Zhang X, Lin J H and Huang F Q 2015 *J. Am. Chem. Soc.* **137** 10148
- [15] Coldea A I and Watson M D 2018 *Annu. Rev. Condens. Matter Phys.* **9** 125
- [16] Wang Q S, Shen Y, Pan B Y, Zhang X W, Ikeuchi K, Iida K, Christianson A D, Walker H C, Adroja D T, Abdel-Hafiez M, Chen X J, Chareev D A, Vasiliev A N and Zhao J 2016 *Nat. Commun.* **7** 12182
- [17] Wang Q S, Shen Y, Pan B Y, Hao Y Q, Ma M M, Zhou F, Steffens P, Schmalzl K, Forrest T R, Abdel-Hafiez M, Chen X J, Chareev D A, Vasiliev A N, Bourges P, Sidis Y, Cao H B and Zhao J 2016 *Nat. Mater.* **15** 159
- [18] Rahn M C, Ewings R A, Sedlmaier S J, Clarke S J and Boothroyd A T 2015 *Phys. Rev. B* **91** 180501(R)
- [19] Chen T, Chen Y Z, Kreisler A, Lu X Y, Schneidewind A, Qiu Y M, Park J T, Perring T G, Stewart J R, Cao H B, Zhang R, Li Y, Rong Y, Wei Y, Andersen B M, Hirschfeld P J, Broholm C and Dai P C 2019 *Nat. Mater.* **18** 709

- [20] Yuan D N, Yuan J, Huang Y L, Ni S L, Feng Z P, Zhou H X, Mao Y Y, Jin K, Zhang G M, Dong X L, Zhou F and Zhao Z X 2016 *Phys. Rev. B* **94** 060506(R)
- [21] He M Q, Wang L R, Hardy F, Xu L P, Wolf T, Adelman P and Meingast C 2018 *Phys. Rev. B* **97** 104107
- [22] Li J, Lei B, Zhao D, Nie L P, Song D W, Zheng L X, Li S J, Kang B L, Luo X G, Wu T and Chen X H 2020 *Phys. Rev. X* **10** 011034
- [23] Rhodes L C, Böker J, Müller M A, Eschrig M and Eremin I M 2021 *npj Quantum Mater.* **6** 45
- [24] Ma M W, Bourges P, Sidis Y, Xu Y, Li S Y, Hu B Y, Li J R, Wang F and Li Y 2017 *Phys. Rev. X* **7** 021025
- [25] Liu S B, Yuan J, Huh S, Ryu H, Ma M W, Hu W, Li D, Ma S, Ni S L, Shen P P, Jin K, Yu L, Kim C Y, Zhou F, Dong X L and Zhao Z X 2020 *arXiv* 2009.13286
- [26] Liu S B, Ma S, Wang Z S, Hu W, Li Z A, Liang Q M, Wang H, Zhang Y H, W. L Z Y, Yuan J, Jin K, Li J-Q, Pi L, Yu L, Zhou F, Dong X L and Zhao Z X 2021 *Chin. Phys. Lett.* **38** 057401
- [27] Chen G F, Li Z, Dong J, Li G, Hu W Z, Zhang X D, Song X H, Zheng P, Wang N L and Luo J L 2008 *Phys. Rev. B* **78** 224512
- [28] Wang X F, Wu T, Wu G, Liu R H, Chen H, Xie Y L and Chen X H 2009 *New J. Phys.* **11** 045003
- [29] Lin H, Li Y, Deng Q, Xing J, Liu J, Zhu X, Yang H and Wen H-H 2016 *Phys. Rev. B* **93** 144505
- [30] Dai P C 2015 *Rev. Mod. Phys.* **87** 855
- [31] Xu Z J, Wen J S, Xu G Y, Chi S X, Ku W, Gu G and Tranquada J M 2011 *Phys. Rev. B* **84** 052506
- [32] Johnson P D, Yang H B, Rameau J D, Gu G D, Pan Z H, Valla T, Weinert M and Fedorov A V 2015 *Phys. Rev. Lett.* **114** 167001
- [33] Sushkov O P, Oitmaa J and Zheng W H 2001 *Phys. Rev. B* **63** 104420
- [34] Xu C K and Sachdev S 2008 *Nat. Phys.* **4** 898
- [35] Fang C, Yao H, Tsai W F, Hu J P and Kivelson S A 2008 *Phys. Rev. B* **77** 224509
- [36] Jiang H C, Krüger F, Moore J E, Sheng D N, Zaanen J and Weng Z Y 2009 *Phys. Rev. B* **79** 174409
- [37] Cao H Y, Chen S Y, Xiang H J and Gong X G 2015 *Phys. Rev. B* **91** 020504(R)
- [38] Yu R and Si Q 2015 *Phys. Rev. Lett.* **115** 116401
- [39] Wang F, Kivelson S A and Lee D-H 2015 *Nat. Phys.* **11** 959
- [40] Sato Y, Kasahara S, Taniguchi T, Xing X, Kasahara Y, Tokiwa Y, Yamakawa Y, Kontani H, Shibauchi T and Matsuda Y 2018 *Proc. Natl. Acad. Sci. USA* **115** 1227
- [41] Ye Z R, Zhang Y, Chen F, Xu M, Jiang J, Niu X H, Wen C H P, Xing L Y, Wang X C, Jin C Q, Xie B P and Feng D L 2014 *Phys. Rev. X* **4** 031041
- [42] Miao J, Niu X H, Xu D F, Yao Q, Chen Q Y, Ying T P, Li S Y, Fang Y F, Zhang J C, Ideta S, Tanaka K, Xie B P, Feng D L and Chen F 2017 *Phys. Rev. B* **95** 205127
- [43] Pan B, Shen Y, Hu D, Feng Y, Park J T, Christianson A D, Wang Q, Hao Y, Wo H, Yin Z, Maier T A and Zhao J 2017 *Nat. Commun.* **8** 123
- [44] Ma M W, Wang L C, Bourges P, Sidis Y, Danilkin S and Li Y 2017 *Phys. Rev. B* **95** 100504(R)
- [45] Yi M, Wang M, Kemper A F, Mo S K, Hussain Z, Bourret-Courchesne E, Lanzara A, Hashimoto M, Lu D H, Shen Z X and Birgeneau R J 2015 *Phys. Rev. Lett.* **115** 256403
- [46] Ni S L, Sun J P, Liu S B, Yuan J, Yu L, Ma M W, Zhang L, Pi L, Zheng P, Shen P P, Li D, Shi D E, Li G B, Sun J L, Zhang G M, Jin K, Cheng J G, Zhou F, Dong X L and Zhao Z X 2019 *arXiv* 1912.12614
- [47] Dong X L, Zhou F and Zhao Z X 2020 *Front. Phys.* **8** 586182

Supplemental Material for

**Magnetic-Field-Induced Spin Nematicity in FeSe_{1-x}S_x and FeSe_{1-y}Te_y
Superconductor Systems**

Shaobo Liu, Jie Yuan, Sheng Ma, Zouyouwei Lu, Yuhang Zhang, Mingwei Ma, Hua Zhang, Kui Jin, Li Yu, Fang Zhou*, Xiaoli Dong*, and Zhongxian Zhao

* Correspondence to: fzhou@iphy.ac.cn (F.Z.); dong@iphy.ac.cn (X.D.)

This file includes the following supplemental figures:

Figure S1: Property characterizations of FeS single crystal grown hydrothermally

Figure S2: Temperature-dependent in-plane resistivity and the first derivative for parent Fe_{1.19}Te

Figure S3: The x-ray ϕ scans for FeSe_{1-x}S_x ($x = 0.07$) and FeSe_{1-y}Te_y ($y = 0.06, 1$)

Figure S4: Towfold-anisotropic $\Delta R(\theta, T)/R_{\min}(T)$ measured on the same FeSe sample with three different current directions ($\alpha = 0^\circ, 22^\circ, 90^\circ$)

Figure S5: Field dependences of the maximum $\Delta R(T)/R_{\min}(T)$ at given $T < T_{\text{sn}}$ for nematic FeSe_{0.87}S_{0.13}

Figure S1

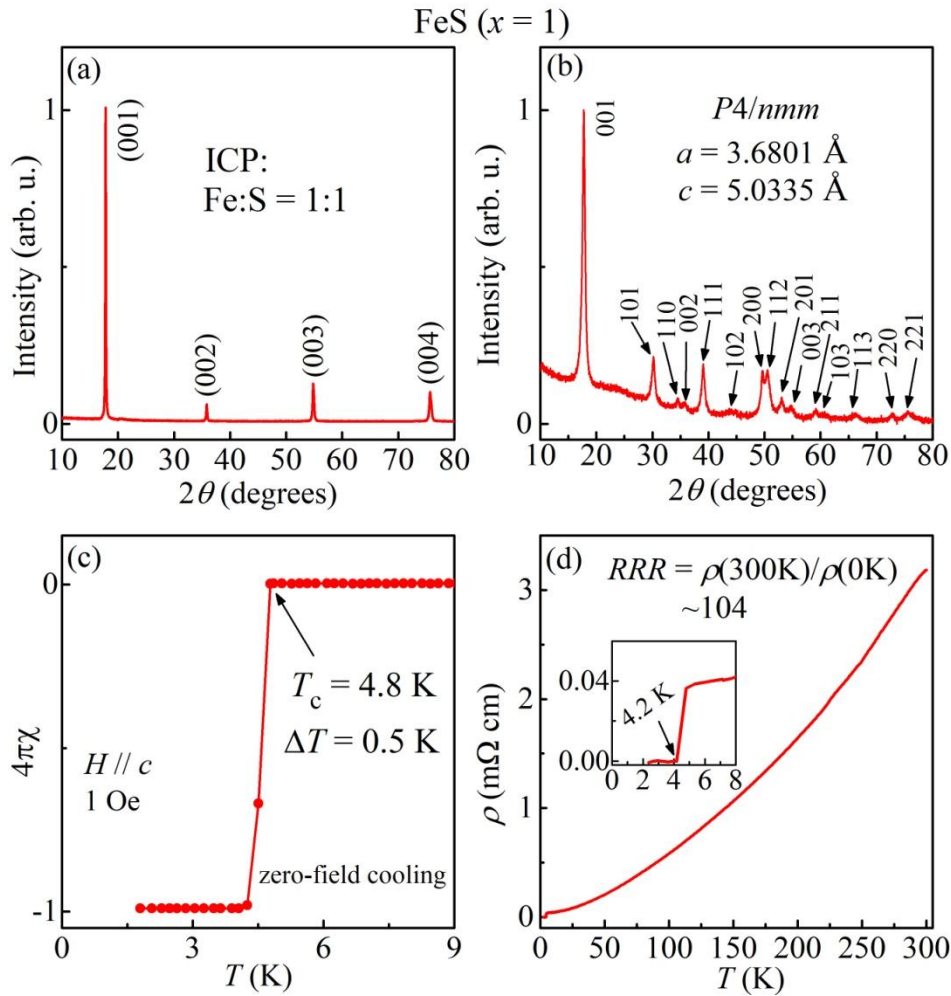


Fig. S1. (a) The single-crystal XRD pattern of FeS sample demonstrates its single preferred (001) crystal orientation. Its chemical stoichiometry is determined by ICP analysis. Both the single-crystal and powder (b) XRD patterns at room temperature confirm the tetragonal crystal symmetry. The calculated lattice constants, a and c , of FeS are the smallest among the $\text{FeSe}_{1-x}\text{S}_x$ and $\text{FeSe}_{1-y}\text{Te}_y$ systems^[25], consistent with previous reports. The superconductivity is characterized by both diamagnetism (c) and resistivity (d) measurements.

Figure S2

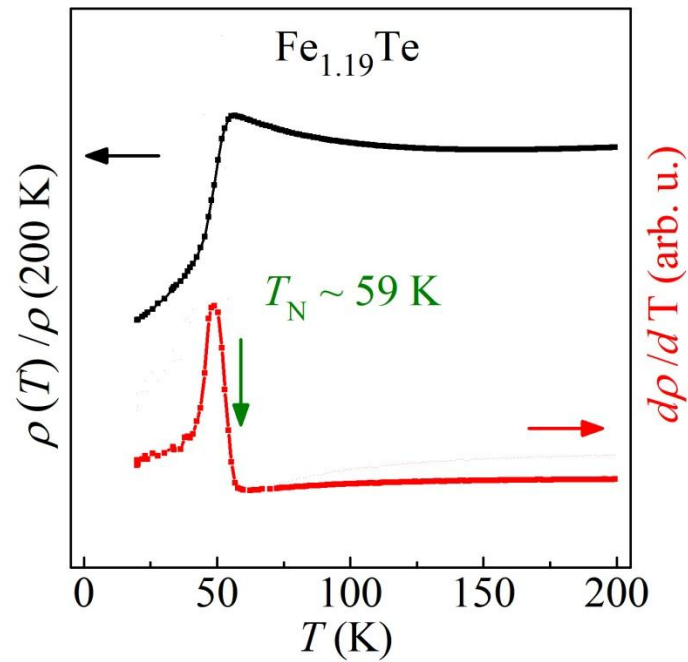


Fig. S2. The temperature-dependent scaled in-plane resistivity and the first derivative of parent $\text{Fe}_{1.19}\text{Te}$ show the pronounced anomaly at $T_N \sim 59$ K.

Figure S3

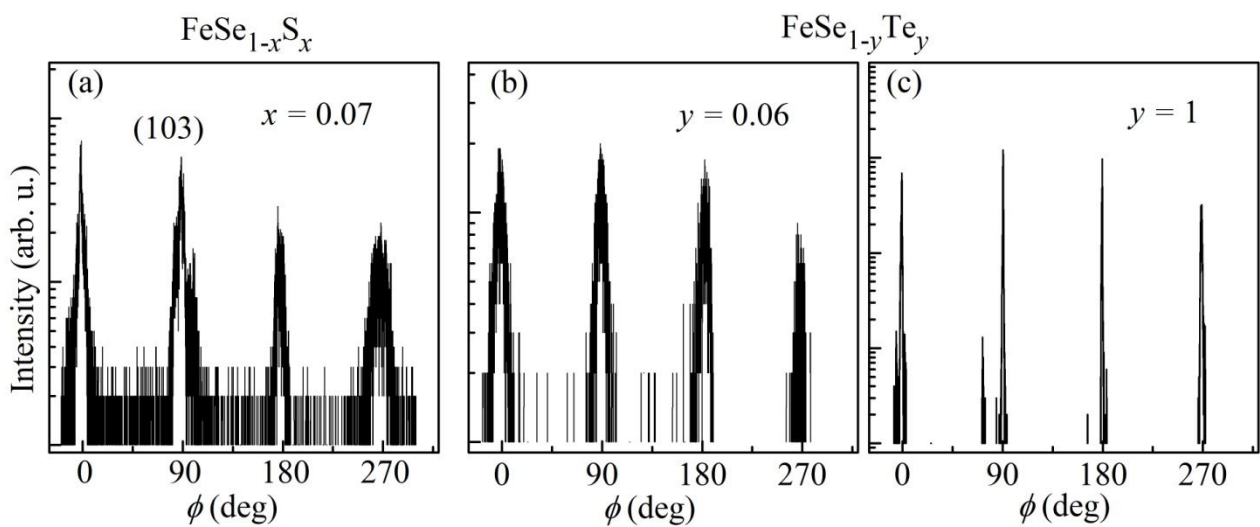


Fig. S3. The room-temperature x-ray ϕ scans of (103) plane for (a) $x = 0.07$ $\text{FeSe}_{1-x}\text{S}_x$, (b) $y = 0.06$ and (c) $y = 1$ $\text{FeSe}_{1-y}\text{Te}_y$ samples.

Figure S4

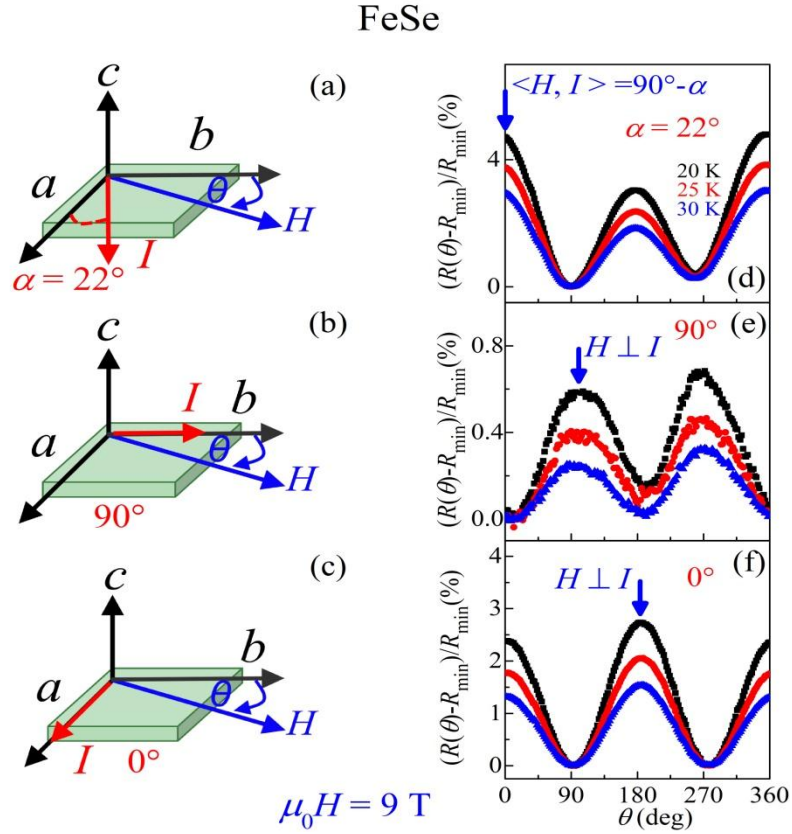


Fig. S4. (a-c) Illustrations of three different current directions (α 's) used in the AMR measurements on the same FeSe sample with $T_{\text{sn}} \sim 90 \text{ K}$. (d-f) The corresponding twofold-symmetric $\Delta R(\theta, T)/R_{\min}(T)$ of the sample measured under magnetic field of 9 T at $T = 20 \text{ K}$, 25 K and 30 K.

Figure S5

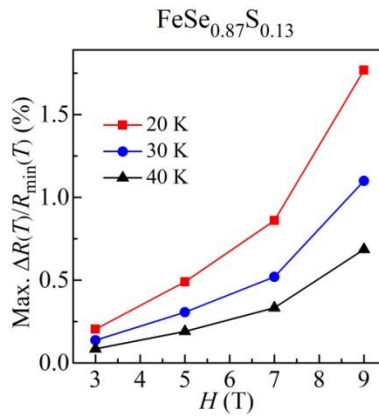


Fig. S5. Field dependences of the maximum $\Delta R(T)/R_{\min}(T)$ at $T = 20 \text{ K}$, 30 K and 40 K for nematic FeSe_{0.87}S_{0.13} ($x = 0.13$) with $T_{\text{sn}} \sim 90 \text{ K}$. The data are extracted from Fig. 3(h) in the main text.